Reducing Radar Cross Section While Keeping the Performance of a CPW-fed Antenna with an Absorptive Metasurface

Humberto Fernández-Álvarez[1], María Elena de Cos Gómez[1] and Fernando Las-Heras Andrés[1]

[1] Department of Electrical Engineering, University of Oviedo, Gijon, Spain.
E-mail: uo194342@uniovi.es

Received xxxxxx
Accepted for publication xxxxxx
Published xxxxxx

Abstract

The paper presents for the first time an analysis on the optimum arrangement of a CPW-fed monopole antenna and a metasurface absorber (MSA), aiming at reducing the antenna's in-band Radar Cross Section (RCS) without perturbing its radiation properties. The proposed arrangement will show that the efficiency of the antenna, of great interest in many applications (such as IoT), can be preserved, contrary to what happens in previous papers focused on combining these structures. Moreover, the final structure will be easily embeddable (with an optimum number of unit-cells) as well as conformable. A proper analysis of the losses and currents on the structure will be provided for better understanding the interaction phenomena that arise. Good agreement between simulation and measurement results can be observed, corroborating the proper performance of the structure. Furthermore, not only monostatic RCS reduction but also bistatic one is obtained, due to the angular stability of the employed MSA. Finally, it will be shown that the introduction of loaded resistors will be preferable than the use of a lossy dielectric to improve the RCS reduction whilst keeping the antenna performance.

Keywords: Angular stability, CPW-fed antenna, metasurface, microwave absorbers, radar cross section reduction, ultrathin antenna.

1. Introduction

During the recent years, many authors have focused their studies on metamaterials, which are three-dimensional periodic structures exhibiting properties not found in natural materials. Metamaterials have been employed in a great amount of applications such as cloaking and shielding for concealing objects [1]-[3], imaging to increase the electromagnetic image resolution [4] or sensing [5] among others. Metasurfaces are two-dimensional periodic metamaterials, which have been mainly designed to reflect or guide electromagnetic waves as desired [6]-[9]. They have been widely investigated due to their ability to reduce the Radar Cross Section (RCS) of electromagnetic devices, especially antennas [10]-[25]. Different types of metasurfaces such as Frequency Selective Surfaces (FSSs) [10], Partially Reflective Surfaces (PRSs) [11]-[12], Metamaterial Polarization Converters [13], checkerboard arranged Artificial Magnetic Conductors (AMCs) [14]-[15], coding metasurfaces [16]-[18] and Metasurface Absorbers (MSAs) [19]-[27] have been combined with antennas with the aforementioned goal.

To compute the RCS reduction of an antenna two modes have to be considered: structural and antenna ones. The former

(structural mode) comes from the scattering of its geometry and substrate properties and the latter (antenna mode) is caused by the mismatch at the antenna port, which may give rise to re-radiation. It should be mentioned that this re-radiation is minimized or even removed when the antenna is matched to the port, since there will be no reflection on it. In this case, just the structural mode has to be analyzed [28].

As it is mentioned in [11], most literature contributions on combining antennas with MSAs are focused on reducing the out of band RCS. For example, when FSSs are designed as antennas radomes, they usually transmit electromagnetic waves within the antenna's operating band and absorb the incoming waves out of this band. Other literature contributions combine antennas with PRSs [11]-[12], [29]. However, the latter gives rise to large thicknesses and non-conformable structures. Checkerboard arranged AMCs and coding metasurfaces are based on scattering the incoming wave in different directions, causing a destructive interference of the backscattered wave. Although they highly reduce the RCS in the backscattered direction and/or specular one, they require many unit-cells for doing so and hence, it is not appropriate for applications with size restrictions. Moreover, the design procedure is usually time consuming as it involves an optimization process and it is usually designed to operate under normal incidence and certain polarization angle, degrading its performance for other incidence and/or polarization angles [30]. Other common issues are the use of lossy dielectrics, such as the FR4, which deteriorate the antenna's performance and the consideration of many unit-cells giving rise to large profiles. Moreover, in many papers either just the monostatic RCS reduction is taken into account [22], [31] or when additionally considering the bistatic one, it is just calculated for certain angles [19], [23]. The latter are some of the issues that one can commonly encounter in literature contributions.

In this paper, a study on the best combination of a CPW-fed monopole antenna and a MSA will be conducted aiming at reducing the monostatic and bistatic in-band RCS, without deteriorating the antenna's performance. Although there are several papers on combining antennas with MSAs, as it was previously mentioned, from the author's best knowledge it is the first time that a CPW-fed monopole antenna is considered and all the mentioned goals are achieved, which are commonly a drawback in many literature contributions. Indeed, it will be shown that both the in-band RCS can be reduced and the antenna's parameters will be kept by properly designing and arranging both structures, contrary to what happen in most literature contributions [29], [31]-[34]. In fact, this paper will show how to preserve the antenna radiation properties, by means of a reasonable current and loss analysis of the MSA and antenna, when both operates at the same frequency. Therefore, it does not only aim at introducing a new antenna-MSA structure, but also giving the keys for their optimum combination. Additionally, it will be shown that the introduction of lumped resistors to further reduce the antenna RCS provides similar conclusions.

2. Design description

The CPW-fed monopole antenna, presented in Figure 1(a), will be combined with an MSA aiming at reducing the antenna's RCS. The MSA will be the same as the one presented in a previous contribution published by the authors of this paper [35], having the following geometrical dimensions: $p_1 = 14.4\,mm$, $p_2 = 13.7\,mm$, $h_e = 2\,mm$, $h_i = 1\,mm$, , $w = 0.32\,mm$ and $l = 6.2\,mm$ (see Figure 1). It is designed on a commercially available 0.457mm thickness Arlon25N dielectric and it exhibits an absorption peak of 88% at its resonance frequency (6.3 GHz). The antenna is devised to resonate around the MSA's resonance frequency and using the same dielectric with identical thickness. To fulfil the previous requirements, it should have the following dimensions: $L_{ant} = 19.2\,mm$, $W_{ant} = 14.7\,mm$ $L_g = 8.5\,mm$, $L_p = 6.7\,mm$, $A_L = 1\,mm$, $A_w = 4\,mm$, $w = 4\,mm$ and $g = 0.23\,mm$.

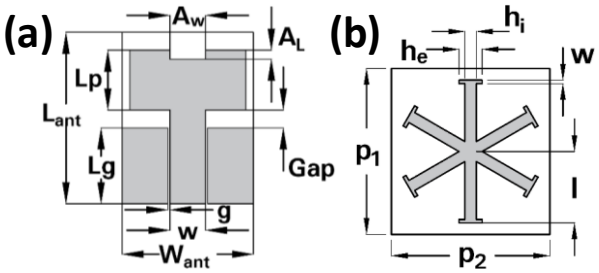

Figure 1. (a) CPW-fed monopole antenna. (b) MSA's unit-cell geometry.

3. Results

The antenna and several MSAs were manufactured using a laser micromachining technology with a LPKF Protolaser-S machine.

1.1 CPW-fed monopole antenna measurements

The manufactured antenna (UMA), with the aforementioned parameters, is presented in Figure 2(a). Then, its S11 parameter was measured employing a VNA. A comparison between the simulation and measurement results of the UMA is presented in Figure 2(b). It should be noticed that the antenna is well matched in both simulation and measurements. The observed discrepancies are mainly attributed to the absence of the connector in simulation and the cable's effect in measurements. Indeed, the ground plane is considerably small and it is part of the radiant structure. Consequently, the measurement cable's head may perturb the

currents distribution on its ground plane. Similar discrepancies have been found in other papers when measuring such small antennas [36]-[38]. After several simulations, it was concluded that the soldering inclusions, which partially enter the gap between the antenna feeding strip line and its ground plane, are the main reason for the presence of the additional peak between 9 GHz and 10 GHz. Other discrepancies come from manufacturing tolerances, discrepancies in the dielectric properties and errors in fixing the optimum time window (when using time gating to avoid undesirable effects). Nevertheless, it should be noticed that in an actual application, these discrepancies will not appear, since the antenna and the MSA will be integrated in a system and the effect of the connector and soldering inclusions will not exist.

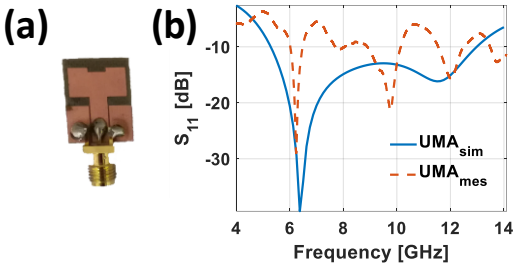

Figure 2. CPW-fed monopole antenna: (a) manufactured prototype, (b) simulation vs measurement S11 results.

1.2 CPW-fed monopole antenna combined with the MSA

Then, keeping the previous parameters for both the antenna and the MSA, they are combined and two cases are analyzed. Antenna and MSA: with a foam layer in between of hfoam = 4.14 mm (UMAF) (see Figure 3(a)) and in the same layer sharing the dielectric (UMASL) (see Figure 3(b)). It should be noticed that many applications have size restrictions and hence, the number of unit-cells has to be minimized so that the structure still behave as a MSA. Different MSAs, on which the number of unit-cells is varied, have been analyzed. For the sake of compactness, in this paper, it is chosen to show the results of combining the antenna with MSAs, which have the smallest number of unit-cells that provides a suitable explanation of the interaction phenomena between both. By considering a large number of unit-cells, similar conclusions in terms of antenna's performance can be extracted. The simulation and measurement results are presented in Figure 4 for both the UMAF and UMASL. To avoid the connector effects, the measurements are firstly visualized in the time domain. The latter allows to apply a time window (time gating procedure) to select the reflection from the antenna and filter the one from the connector. Then, a Fourier Transformation is applied to the windowed time signal to obtain the matching results of the antenna in Figure 4. Similar discrepancies can be noticed between simulation and measurements, which can be attributable to the same reasons given above for the UMA.

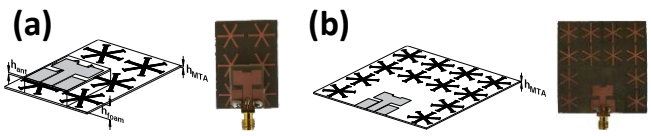

Figure 3. CPW-fed monopole antenna combined with the MSA: (a) with a foam layer in between (UMAF), (b) in the same layer sharing the dielectric (UMASL).

The bandwidth (BW) and radiation parameters (Directivity (D), Gain (G), radiation efficiency (η) and front to back ratio (F/B)) of the UMA, UMAF and UMASL at their resonance frequencies (f_r) are extracted from the simulation software and gathered in Table 1. One can notice that the UMASL clearly outperforms the radiation parameters of the UMA or at least keeps them. On the other hand, the UMAF exhibits a poor efficiency in the lower band, as the MSA is absorbing part of the antenna's radiation and it increases in the upper band, since the MSA is acting as a Perfect Conductor (PEC) a quarter wavelength from the antenna. On the other hand, the UMAF exhibits a large thickness and the matching properties between both resonances are lost, as one can see from the simulation results in Figure 4(a). Therefore, for the sake of compactness, it will be discarded in the subsequent comparisons, due to its worse overall performance in terms of efficiency and impedance matching.

On the other hand, when the antenna shares the same dielectric with the MSA (UMASL), the resulting structure can be considered as conformable, owing to the small thickness and flexural strength of the considered dielectric.

It can be noticed that the unit-cells, when comparing the UMAF and UMASL (see Figure 3), exhibit a rotated orientation. However, similar conclusions can be extracted when considering non-rotated unit-cells, except for a slight shifting of the first resonance frequency.

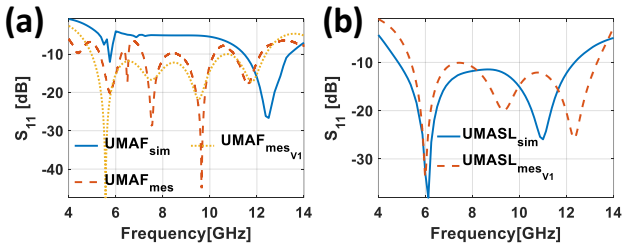

Figure 4. Simulation vs measurement S11 with different time windows: (a) UMAF and (b) UMASL.

The radiation patterns at the lower resonance frequencies of the UMA and UMASL are presented in Figure 5 in the E- and H-planes. It should be mentioned that, in this band, the MSA is operating. It can be noticed similar radiation patterns for both antennas, which confirm that the MSA is not affecting the antenna radiation when operating in the same band. The only difference comes from the cross-polar component, especially in the H-plane, which is slightly higher in the UMASL, but it is still low. Indeed, it is known that the cross-

polarization level of an antenna may increase when adding parasitic inclusions to it, as they also contribute to its radiation pattern. The latter also happens when adding whatever other metasurface surrounding the antenna that contributes to its radiation. However, although this level is increased, it is 15dB below the co-polar component, which is a reasonable level for most applications. Therefore, one can conclude that the combination of the antenna with the MSA on the same layer preserves not only the radiation properties, but also the radiation pattern shapes.

	UMA		UMAF		UMASL	
f_r [GHz]	6.38	11.63	5.75	12.5	6.13	11
S_{11} [dB]	-39.4	-16.2	-12.1	-26.7	-38.1	-26
BW [MHz]	7690	7690	80	1930	7510	7510
D [dBi]	2.6	5.6	6.7	10.34	4.04	8
G [dB]	2.5	5.5	5	10.3	3.98	7.99
η [%]	99	99	67.7	99	99	99
F/B [dB]	0.1	2.6	15.9	13.7	3.7	1.7

Table 1. Comparison between the UMA, UMAF and UMASL in terms of radiation parameters and bandwidth.

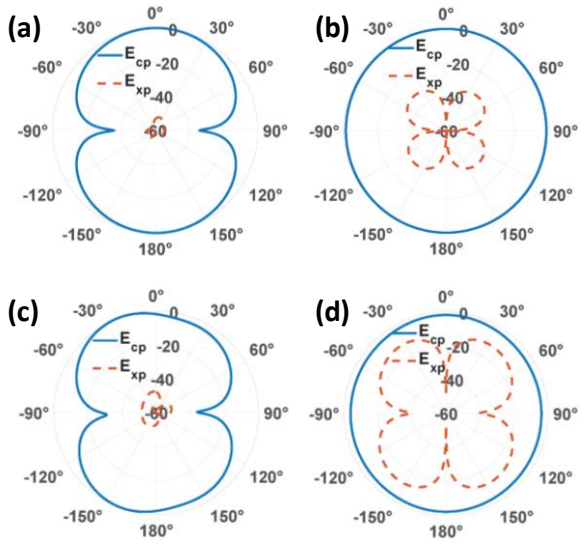

Figure 5. Simulated radiation patterns at the lower resonance frequency of the (a,b) UMA (at its f_r (6.38 GHz)) and (c,d) UMASL (at its f_r (6.13 GHz)) in the E- and H-plane.

For a better clarification on the matching discrepancies between the simulation and measurement results, the soldering inclusions were added to the simulation of the UMASL and the results are shown in Figure 6. The additional peak observed in the measurement results is also clearly noticed in the simulation result. Therefore, one can conclude that the differences between the simulation and measurement results observed in Figure 4 are mainly due to the soldering inclusions. The same conclusion can be applied to the results presented in Figure 2.

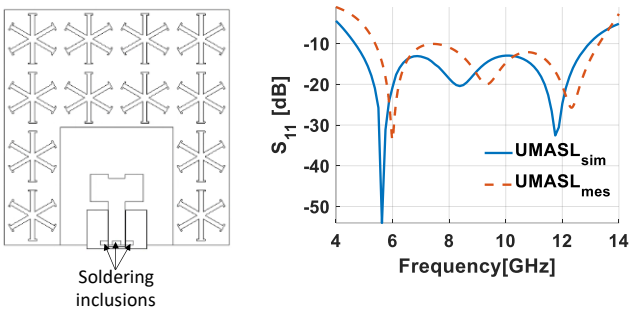

Figure 6. (a) UMASL with the soldering inclusions. (b) Simulation vs measurement S11 results of the UMASL when considering the soldering inclusions.

1.3 Loss power densities in the UMA and UMASL

In this section, the loss power is computed for both the UMAF and UMASL aiming at clarifying the previous conjectures about the radiation efficiency of the structures. Therefore, the volume loss density will be computed in both structures as follows:

$$\rho_{loss} = \frac{1}{2} Re\{E \cdot J^*\} \quad (1)$$

This quantity is depicted in Figure 7, for both UMAF and UMASL at their respective resonance frequencies (see Table 1). As one can clearly notice, the absorption is clearly large for the UMAF at its lower resonance frequency (see Figure 7(a)). This is why the radiation efficiency of the antenna is deteriorated. The latter statement confirms what was speculated in the previous section, regarding the UMAF efficiency. On the other hand, in the UMASL there are almost no power loss in the lower band (Figure 7(c)) and this is why the radiation efficiency keeps unaltered (see Table 1). Finally, it should be mentioned that in the upper band the MSA does not perturb the radiation efficiency of the antenna, since almost no absorption can be observed in both the UMAF and UMASL (see Figure 7(b) and (d)). Therefore, aiming at using a MSA working in the same frequency band as the antenna, the better choice is to arrange it in the same plane, so that it does not perturb the antenna radiation properties, whereas, as it will be shown latter, it reduces the RCS.

1.4 Surface current distribution on the UMA and UMASL

The surface current of both the UMA and UMASL is presented in a vectorial form in Figure 8 at their respective resonance frequencies. One can observe that this current distribution keeps unaltered, when introducing the MSA surrounding the antenna. Therefore, this provides certain evidences to foresee that the radiation properties of the antenna, with and without the MSA surrounding it, will be kept unaltered. Moreover, the currents excitation on the unit-cell's metallization gives rise to an extra forward constructive

contribution to the main lobe radiation of the antenna (as the one provided by a parasitic copper sheet element) and an improvement of antenna's gain.

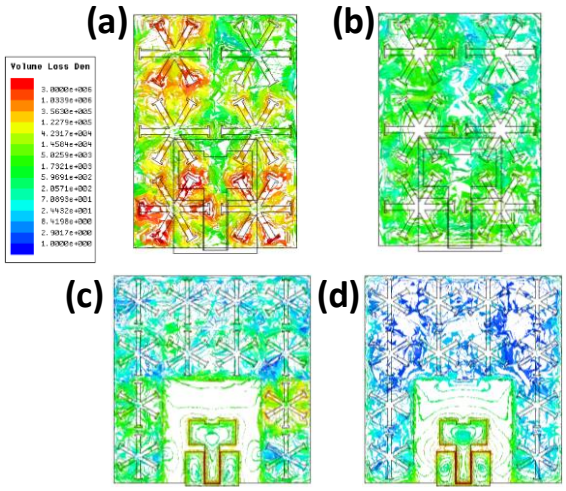

Figure 7. Volume loss density of the UMAF ((a) 5.75 GHz and (b) 12.5 GHz) and UMASL ((c) 6.13 GHz and (d) 11 GHz) at their respective resonance frequencies.

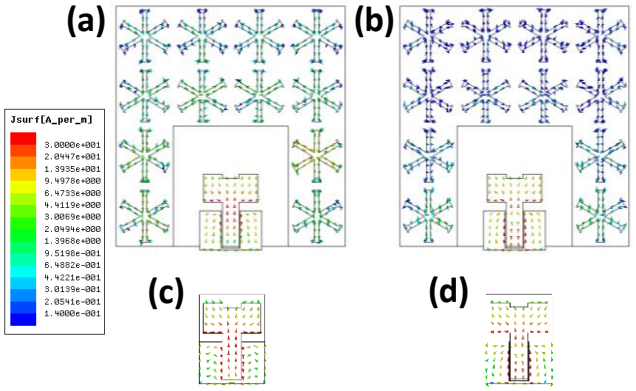

Figure 8. Surface current of the UMASL ((a) 6.13 GHz and (b) 11 GHz) and UMA at their respective resonance frequencies.

1.5 Simulation vs measurements of the UMA and UMASL

Aiming to conduct a fair comparison between the UMA and the UMASL, they should be compared at the same frequency and under similar impedance matching. Therefore, the measurements are conducted in an anechoic chamber at 9.6 GHz (see Figure 9). The directivity, gain and efficiency are computed from the simulation and measurement results and they are presented in Table 2. From the measurement results, the directivity is calculated by integrating the measured 3D radiation pattern and the gain is computed using the gain transfer method.

	UMA		UMASL	
	Sim	**Meas**	**Sim**	**Meas**
D [dBi]	4.5	4	7	6.5
G [dB]	4.3	3.7	6.8	6.2
η [%]	95.4	92.9	94.1	92.7

Table 2. Comparison between the radiation patterns of UMA and UMASL computed from the simulation and measurement results at 9.6 GHz.

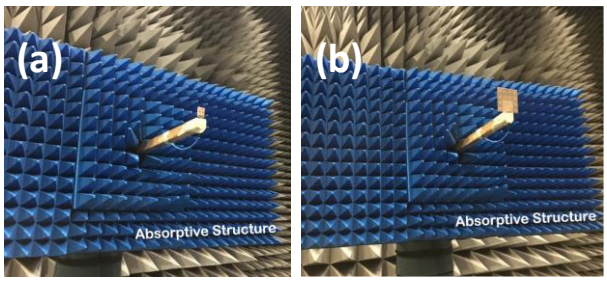

Figure 9. UMA and UMASL on the positioner.

Moreover, the simulated and measured radiation patterns in the E- and H-planes are presented in Figure 10 and Figure 11 for the UMA and UMASL, respectively. Good agreement can be noticed between both results. The slight discrepancies observed around a 90º azimuth angle are mainly due to the influence of the absorptive structure (used to avoid possible interactions between the pylon and the antenna (see Figure 9)) and the impracticability of placing the antenna on its phase center (due to the anechoic chamber configuration). Moreover, the differences in the cross-polar component in the E-plane are mainly attributable to the available dynamic range, which is low for measuring such a small cross-polar level values obtained through simulation. Therefore, it can be concluded that the behavior of the previous structures has been validated not only from simulation but also from measurement results.

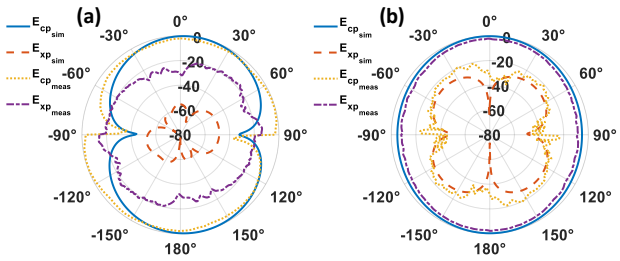

Figure 10. Simulated (sim) and measured (meas) radiation patterns of the UMA at 9.6 GHz in the (a) E- and (b) H-plane.

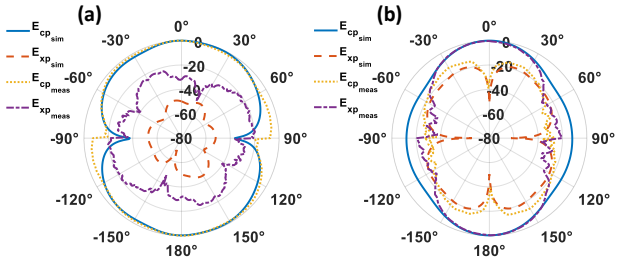

Figure 11. Simulated (sim) and measured (meas) radiation patterns of the UMASL at 9.6 GHz in the (a) E- and (b) H-plane.

1.6 RCS reduction of the UMASL

Once it was shown that the radiation pattern of the UMA is not deteriorated when it is combined with the MSA in the same layer (UMASL), its RCS is analyzed. For conducting a proper study of the RCS reduction (RCSr) (see Figure 12), a normalization step is necessary. Therefore, the RCS of the UMASL is normalized by the one of a similar antenna, on which its unit-cells metallizations are replaced by a metallic plate (see Figure 12(d)). The latter provides a fair comparison, since both structures have not only identical size, but also and more important similar radiation properties, which is not achieved by barely enlarging the antenna size (without introducing the parasitic metallic plate). Indeed, it should be noticed that in most actual applications, the antenna will be assembled in a device or system which has probably different metallic parts. In Figure 12(b) and (c), the incident plane (transmitting antenna position) and the reflected one (receiving antenna position) are respectively rendered. Moreover, for considering both transverse electric (TE) and transverse magnetic (TM) polarizations, the electric field should be polarized in the ϕ and θ directions of the spherical coordinate reference system, respectively.

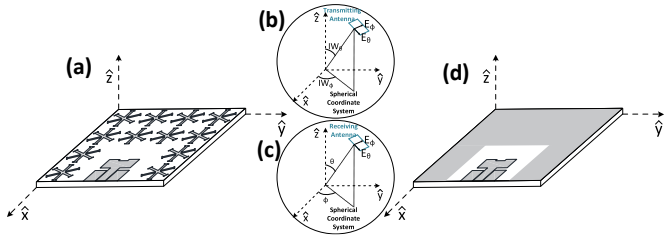

Figure 12. (a) UMASL, (b) incident plane and (c) reflected plane. (d) UMASL on which its unit-cells metallizations are replaced by a copper sheet.

The normalized monostatic RCS versus frequency is analyzed under normal incidence and the results in the planes 0º and 90º for both TE and TM polarizations are presented in Figure 13(a) and (b). One can notice that under normal incidence the ϕ and θ components of the electric field (E_ϕ and E_θ) satisfy the following relations: $E_\phi|_{IW_\phi=0^\circ} = E_\theta|_{IW_\phi=90^\circ}$ and $E_\phi|_{IW_\phi=90^\circ} = E_\theta|_{IW_\phi=0^\circ}$. Therefore, under normal incidence identical RCS reduction can be observed for TE and TM polarizations in the planes $IW_\phi = 0^\circ$ and $IW_\phi = 90^\circ$ and vice versa. A clear RCS reduction can be noticed around the MSA's resonance frequency (at slightly lower frequency due to the influence of both: the consideration of a finite structure and the antenna). Indeed, more than half of the energy is absorbed by considering just 12 unit-cells and without increasing the antenna's thickness.

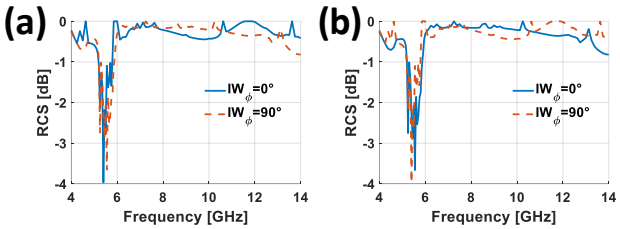

Figure 13. Normalized monostatic RCS versus frequency in the planes 0º and 90º for both (a) TE and (b) TM polarizations.

The normalized bistatic RCS is also computed when the transmitting and receiving antennas are at different positions and at the frequency on which high RCS reduction is observed from the monostatic results (5.55 GHz (see Figure 13)). Moreover, both TE and TM polarizations in the planes $IW_\phi = \phi = 0^\circ$ and $IW_\phi = \phi = 90^\circ$ are considered. From the results (Figure 14), proper RCS reduction can be clearly noticed, especially at the specular angles ($\theta = -IW_\theta$).

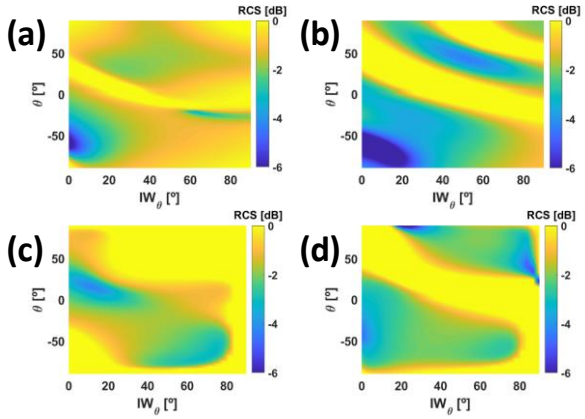

Figure 14. Normalized bistatic RCS of the UMASL, varying the transmitting and receiving antennas position (IW_θ and θ), for both TE and TM polarizations at $IW_\phi = \phi = 0^\circ$ (a,b) and $IW_\phi = \phi = 90^\circ$ (c,d) planes

1.7 RCS reduction of the UMASL_M

Although the previous structures reduce the antenna RCS without deteriorating its performance, it should be noticed that the considered MSA exhibits a high absorption, but as an ultrathin low lossy dielectric was considered,it is not perfect (88%) [35]. Therefore, one may wonder what if a resistor loaded MSA, which exhibits a perfect absortion due to the resistors inclusion, would deteriorate the antenna behavior. Consequently, the previous MSA is slightly modified and some lumped resistors of 0805 case size are added, so that the new MSA is the one presented in Figure 15(a). The unit-cell will have the following parameters: $p = 11.5\,mm$, $l_1 = 2.75\,mm$, $l_2 = 1.55\,mm$, $l_R = 1.2\,mm$, $h_i = 1.4\,mm$, w = 0.3 mm, $w_R = 1.2\,mm$, and $\alpha = 56^\circ$. The lumped resistor value will be 0.3 Ω to attain perfect absorption. This MSA exhibits a perfect absorption around 6 GHz and a bandwidth (FWHM) of 3.42%, which is larger than the one of the

previously presented MSA. In addition, the unit-cell has also been miniaturized due to an increase on its capacitive behavior. Then, the new MSA is combined with the same antenna used in the previous sections (UMA), resulting in the UMASL_M (see Figure 15(b)). As in the previos comparison, the monostatic RCS of the UMASL_M is similarly normalized using the structure in Figure 15(c) (UMASL_Mref). From Figure 16(a), a large RCS reduction around 6.3 GHz with a -3 dB RCS reduction of 180 MHz and peaks of -9.1 dB and -15.35 dB respectively in the planes 0º and 90º can be noticed.

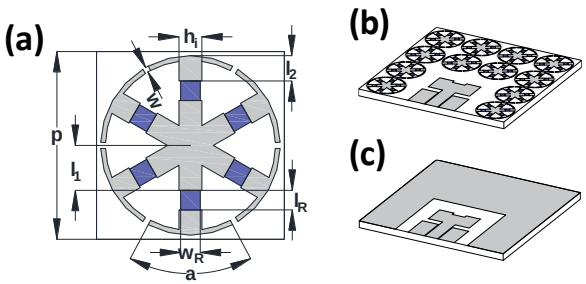

Figure 15. (a) New MSA's unit-cell geometry, (b) UMASL_M and (c) UMASL_Mref.

Moreover, the radiation properties of the antenna are analyzed. The matching properties are depicted in Figure 16(b) and the radiation parameters presented in Table 3. One can notice that the performance of the antenna is slightly improved or at least kept as compared with the reference one. Moreover, the antenna bandwidth is slightly increased with respect to the UMA, since the MSA unit-cells are slightly smaller than the ones previously considered and hence they are closer to the antenna [40]. Consequently, it can be concluded that the introduction of the lumped resistors in the MSA unit-cells does not perturb the antenna performance and as a reward the new MSA further reduces the RCS.

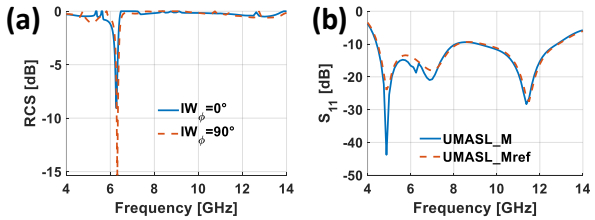

Figure 16. (a) Normalized monostatic RCS versus frequency in the planes 0º and 90º and S11 results of the UMASL_M and UMASL_Mref.

	UMASL_M		UMASL_Mref	
f_r [GHz]	4.87	11.37	4,87	11.5
S_{11} [dB]	-43.7	-28.33	-23.97	-27.4
BW [MHz]	8380	8380	8380	8380
D [dBi]	4.58	6.67	4.32	6.29
G [dB]	4.55	6.67	4.26	6.29
η [%]	99	100	99	100
F/B [dB]	1.34	0.77	0.97	0.52

Table 3. Comparison between the UMA, UMAF and UMASL in terms of radiation and bandwidth.

4. Discussion

From the previous results, it follows that most of the limitations that arise when combining antennas with MSAs mentioned in the introduction (radiation properties deterioration, large profile, lack of conformability and just monostatic analysis) have been overcome in at least two of the designs that this paper is about. In many papers [31]-[34], it is stated that the antenna's radiation properties are deteriorated when combining an antenna with a radar absorbing material (such as a MSA) operating both in the same frequency band. Nevertheless, in this paper it was shown that when the antenna and the MSA are combined in the same layer, which also makes its fabrication easier, the aforementioned radiation properties deterioration is avoided. Indeed, a proper dielectric with low losses has been chosen to not deteriorate the antenna's efficiency and small thickness and flexural strength to make the structure conformable. Many contributions use a FR4 dielectric [19]-[23], [31] to obtain large absorption, but the latter brings about low antenna's radiation efficiency. Moreover, it was shown that the RCS reduction can be enlarged introducing lumped resistors without deteriorating the antenna performance.

On the other hand, in other works a large number of unit-cells is considered [19]-[20], [22]-[24], [39], which may cause high RCS reduction. However, most applications entail size restrictions, which is taken into account here, by considering just a small number of unit-cells to be combined with the antenna. The latter aims at obtaining an easily embeddable antenna and showing the possible drawbacks, in terms of RCS reduction, that appear when considering a small amount of unit-cells. It should be mentioned that by increasing the number of unit-cells, the RCS reduction could be increased. Another alternative could be the increase of the dielectric thickness at the expense of reducing the conformability of the structure.

Moreover, most papers just consider monostatic RCS reduction [22], [31] or when the bistatic is also taken into account, only a few incidence angles are analyzed [19], [23]. In this study, the structure not only exhibits a proper monostatic RCS reduction but also a bistatic one, due to the angular stability of the MSA. Furthermore, contrary to what happens when considering AMC checkerboard surfaces, when an MSA is considered the energy of the incoming wave is absorbed and hence, it is not scattered in different directions, which makes this structure less detectable to radars.

For a better clarification Table 4 will compare the proposed structures with the previously aforementioned ones presented in the literature.

Ref	Material	Total size	Antenna type	Resonance Frequency (GHz)	Efficiency	IB or OB RCS reduction[1]	Monostatic RCS reduction	Bistatic RCS reduction
[19]	FR4	82.5x82.5x1	Coaxial fed patch	9.15	-	IB	Yes	Yes (but just two
[20]	FR4	120x120x0.5[2]	CP tilted beam	6.25	68%	IB	Yes	No
[21]	FR4	154x154x1	Coaxial fed patch	6.35	-	IB	Yes	No
[22]	FR4	109x109x1	Coaxial fed patch	4.29; 6.49	-[3]	IB	Yes	No
[23]	FR4	135x135x0.5	Waveguide slot	5.55	-[3]	IB	Yes	Yes (but just one
[24]	FR4	660x100x0.9	Guidewave slot array	3.19	-[3]	IB	Yes	Yes (but just two
[31]	FR4	52.5x52.5x0.8	Coaxial fed patch	6.4	52%	OB	Yes	Yes (but just two
[41]	FR4	50x50x0.8	Coaxial fed patch	10.52	≈80%[3]	IB	Yes	Yes (but just two
[42]	RT/duroid 6002	56x56x1.524	Coaxial fed patch	4.5	-	OB	Yes	No
[43]	FR4	πx45x1.5	Coaxial fed circular patch	5.83	<80%	IB	Yes	Yes (but just two planes)
UMASL	Arlon25N	57.6x54.8x0.457	CPW fed monopole	8.63	>92%	IB	Yes	Yes
UMASL_M	Arlon25N	46x46x0.457	CPW fed monopole	8.56	>92%	IB	Yes	Yes

[1] IB and OB stand for in-band and out of band, respectively.
[2] Considering the total thickness of antenna and MSA, it will be 15.1.
[3] Gain reduction.

Table 4. Comparison of the proposed MSA-Antenna with other literature contributions.

As it can be seen from the table, it is the first time that an easily embeddable and conformable structure comprising a MSA and an antenna is presented, showing not only proper monostatic and bistatic in-band RCS reduction, but also no deterioration of the antenna's radiation properties.

5. Conclusion

In this paper, different arrangements of a CPW-fed monopole antenna with MSAs including or not lumped resistors have been analyzed, aiming at finding an optimum configuration. From the analysis, it was reasonably concluded, using not only the retrieved radiation parameter results but also the current and losses in the structure, that the best one is the placement of both structures in the same layer (sharing the dielectric). It was also shown that not only the in-band RCS is reduced, but also the antenna's radiation properties are preserved, using the aforementioned arrangement. Moreover, contrary to what was conducted in many papers, a proper dielectric was selected for designing both the antenna and the MSA, aiming at avoiding the common antenna's radiation properties deterioration and at the same time, making the final structure conformable. The latter was also shown when introducing lumped resistors in the MSA that surrounds the antenna, which also provides a clear increase in the RCS reduction. Therefore, it could be concluded that it is preferable to increase the surface resistance of the MSA combined with an antenna (inserting resistors for example), instead of the dielectric losses, for increasing the RCS reduction of the structure without deteriorating the antenna's performance. Indeed, it was shown for the first time, that the addition of resistors to the MTA's unit-cell metallizations do not deteriorate the antenna's efficiency and provides an extra reduction of the RCS.

On the other hand, a small number of unit-cells have been considered to account for possible applications entailing size constrains. Therefore, the structure can be easily embeddable with other devices or systems.

Finally, a monostatic and bistatic RCS analysis have been conducted and proper results are obtained for both, due to the angular stability of the MSA.

Acknowledgements

This work was supported by Ministerio de Ciencia, Innovación y universidades of Spanish Government under project MILLIHAND RTI2018-095825-B-I00, by the Gobierno del Principado de Asturias and European Union (FEDER) under Project GRUPIN-IDI-2018-000191 and by the Gobierno del Principado de Asturias under the "Severo Ochoa" program of Ayudas predoctorales para la investigación y docencia del Principado de Asturias (grant BP16024).

References

[1] Alù A, and Engheta N 2008 *Phys. Rev. Lett.* **100** 113901.
[2] Alitalo P, Luukkonen O, Jylha L, Venermo J and Tretyakov S A 2008 *IEEE Trans. Antennas Propag.* **56** 416.
[3] R S Schofield et al 2014 *New J. Phys.* **16** 063063.
[4] Mário G Silveirinha et al 2011 *New J. Phys.* **13** 053004
[5] Chen T, Li S and Sun H 2012 *Sensors* **12** 2742.
[6] de Cos M E, Alvarez-Lopez Y and Las Heras F 2010 *Prog. Electromagn. Res.* **107** 147.
[7] Fernández Álvarez H F, de Cos M. E. and Las-Heras F. 2015 *Materials*, **8**, 1666.
[8] Fernández Álvarez H, de Cos M E and Las-Heras F 2018 *IEEE Antennas Wireless Propag. Lett.* **17** 813.
[9] Li W, Zhang Y, Wu T, Cao J, Chen Z and Guan J 2019 *Results Phys.* **12** 1964.
[10] Costa F and Monorchio A *IEEE Trans. Antennas Propag.* **60** 2740.
[11] Pan W, Huang C, Chen P, Ma X, Hu C and Luo X 2014 *IEEE Trans. Antennas Propag.* **62** 945.
[12] Cong LL, Cao XY, Li W and Zhao Y 2016 *Prog. Electromagn. Res* **59** 77.
[13] Liu Y, Hao Y, Li K and Gong S 2016 *IEEE Antennas Wireless Propag. Lett.* **15** 80.
[14] Zhao Y, Cao X, Gao J, Yao X and Liu X 2016 *IEEE Antennas Wireless Propag. Lett.* **15** 290.
[15] Ameri E, Esmaeli SH and Sedighy SH 2018 *AEU-Int. J. Eectron. C.* **93** 150.
[16] Li J, Khan TA, Meng X, Chen J, Peng G, Zhang A 2019 *IET Microw. Antenna P.* **13** 1719.
[17] Rajabalipanah H, Abdolali A 2019 IEEE Antennas Wireless Propag. Lett. 18 1233.

[18] Han L, Liu C, Lu X 2020 *J. Phys. D Appl. Phys.* ***53*** *445107*.
[19] Zhang ZX and Zhang JC, 2016 *Prog. Electromagn. Res. Symp. (PIERS)* 364.
[20] Sijia L, Cao X, Liu T and Yang H 2014 *Radioengineering* **23** 222.
[21] Baskey HB, Jha AK and Akhtar MJ 2014 *IEEE International Microwave and RF Conference (IMaRC)* 104.
[22] Zhang H, Cao XY, Gao J, Yang H and Yang Q 2014 *Prog. Electromagn. Res. Lett.* **44** 35.
[23] Liu T, Cao X, Gao J, Zheng Q, Li W and Yang H 2012 *IEEE Trans. Antennas Propag.* **61** 1479.
[24] Li S, Gao J, Cao X, Zhao Y, Zhang Z and Liu H 2015 *IET Microw. Antenna P.* **9** 399.
[25] Singh D and Srivastava VM 2018 *AEU-Int. J. Eectron. C.* **90** 53.
[26] Cheng Y, He B, Zhao J and Gong R, 2017 *J. Electron. Mater.* **46** 1293.
[27] Cheng Y, Zou Y, Luo H, Chen F and Mao X 2019 *J. Electron. Mater.* **48** 3939.
[28] Liu Y, Fu DM and Gong SX 2003 *J. Electromagnet. Wave.* **17** 1301.
[29] Sharma A, Gangwar D, Kanaujia BK and Dwari S 2019 *Electromagnetics* **39** 120.
[30] Han Z, Song W and Sheng X 2019 *IEEE Trans. Antennas Propag*. **67** 4269.
[31] Shater A and Zarifi D 2017 *Appl. Comput. Electromag*. **32** 135.
[32] Li YQ, Zhang H, Fu YQ and Yuan NC 2008 *IEEE Antennas Wireless Propag. Lett.* **7** 473.
[33] Zhao Y, Gao J, Cao X, Liu T, Xu L, Liu X and Cong L 2017 *IEEE Trans. Antennas Propag.* **65** 943.
[34] Long M, Jiang W and Gong S 2017 *IET Microw. Antenna P.* **11** 705.
[35] Álvarez HF, De Cos ME and Las-Heras F 2015 *Materials* **8** 1590.
[36] Chen ZN, See TS and Qing X 2007 *IEEE Trans. Antennas Propag*. **55** 383.
[37] Hertel TW, 2005 *IEEE Antennas and Propagation Society International Symposium (AP-S)* 524.
[38] Chen ZN, Yang N, Guo YX, Chia MYW 2005 *IEEE Trans. Instrum. Meas.* **54** 1100.
[39] Fu Q, Fan CL, Sijia L, Wang G and Cao XY, 2016 *Radioengineering* **25** 241.
[40] Hadarig RC, De Cos ME and Las-Heras F 2012 *Int. J. Antennas and Propag.* **843754**.
[41] Liu Y and Zhao X 2014 *IEEE Antennas Wireless Propag. Lett.* **13** 1473.
[42] Pazokian M, Komjani N and Karimipour M 2018 *IEEE Antennas Wireless Propag. Lett.* **17** 1382.
[43] Ren J, Gong S and Jiang W 2018 *IEEE Antennas Wireless Propag. Lett.* **17** 102.